

General Formalism of Mass Scaling Approach for Replica-Exchange Molecular Dynamics and its Application*

Tetsuro Nagai[†]

Department of Physics, Graduate School of Science, Nagoya University, Nagoya, Aichi 464-8602, Japan

Replica-exchange molecular dynamics (REMD) has demonstrated its efficiency by combining trajectories of a wide range of temperatures. As an extension of the method, the author formalizes the mass-manipulating replica-exchange molecular dynamics (MMREMD) method that allows for arbitrary mass scaling with respect to temperature and individual particles. The formalism enables the versatile application of mass-scaling approaches to the REMD method. The key change introduced in the novel formalism is the generalized rules for the velocity and momentum scaling after accepted replica-exchange attempts. As an application of this general formalism, the refinement of the viscosity-REMD (V-REMD) method [Nguyen, *The Journal of Chemical Physics* **132**, 144109 (2010)] is presented. Numerical results are provided using a pilot system, demonstrating easier and more optimized applicability of the new version of V-REMD as well as the importance of adherence to the generalized velocity scaling rules. With the new formalism, more sound and efficient simulations will be performed.

1. Introduction

Molecular dynamics (MD) and Monte Carlo (MC) methods are indispensable for the study of biological systems. Nevertheless, insufficient sampling often leads to great difficulties in terms of the accuracy of these simulations. To conquer these difficulties, the generalized-ensemble algorithms have been developed and applied to these systems (for reviews, see, e.g., Refs. 1–4). The methods widely used include the multicanonical algorithm (MUCA),^{5,6} simulated tempering,^{7,8} and the replica-exchange method (REM).^{9,10} Closely related to the MUCA are the Wang–Landau method,^{11,12} statistical temperature methods,^{13–15} and metadynamics.¹⁶ Metadynamics can also be considered as one of the promising approaches collectively termed mean-force dynamics (see Ref. 17 and references therein). Also closely related to the REM is the method in Ref. 18, which is later detailed in Ref. 19. The replica-exchange molecular dynamics (REMD) method²⁰ is the MD version of REM. The REMD method is widely used in biological systems including lipid membranes.²¹ There are attempts of multi-dimensional generalization (see, e.g., Refs. 22–27) including the NPT ensemble^{3,28–31} and the combination of the Tsallis statistics³² with the REM (see, e.g., Ref. 33). Besides, there are promising studies to further enhance this approach (see, e.g., Refs. 34 and 35 for different replica-exchange schemes, Refs. 36–38 for multiscale simulations, and Refs. 39–41 for replica-exchange with solute tempering and flexible tempering).

As the REMD method deals with the velocity or momentum in addition to the coordinate, special care is necessary for these variables. In particular, Sugita and Okamoto²⁰ suggested that the momentum and velocity should be scaled after accepted replica-exchange attempts. Recently, the author and a coworker have suggested that the scaling of velocity can be substituted by the scaling of mass in proportion to temperature,⁴² as this scaling leads to velocity distributions independent of temperature. This method is referred to as the

mass-scaling REMD (MSREMD) method, and the invariant velocity distributions enhance the stability of MD simulations at high temperatures, thereby allowing for longer time steps. We later suggested that a more general formalism is possible, which was called the mass-manipulating REMD (MMREMD) method therein.⁴³ The method enables the full combination of the mass scaling approaches^{44–55} with the REMD method, both of which have demonstrated their great utility. Accordingly, MSREMD can be considered as a preceding special case of MMREMD. A similar approach was demonstrated to be applicable to simulated tempering.⁵⁶ In this paper, on the basis of the general MMREMD approach, we give a significant refinement over the viscosity-REMD (V-REMD) method,⁵¹ which was reported to enhance the sampling efficiency.

This article is organized as follows. In Sect. 2, we shall examine the MMREMD method. After a review of the original V-REMD method, a new version of the V-REMD method is proposed on the basis of the novel formalism. Section 3 is devoted to Results and Discussion. We compare the numerical results between the original V-REMD method and the new version. We establish that the generalized velocity scaling rule introduced by the new formalism is crucial for the correct sampling, especially when frequent replica-exchange attempts are performed to ensure sampling efficiency as per Refs. 57–59. Thereby, the new formalism equips the V-REMD method to achieve more enhanced performance. Conclusions are given in Sect. 4.

2. Model and Methods

2.1 General formalism of mass scaling in REMD

The MMREMD method is the generalized version of the REMD method.^{9,20} For further details about the REM and REMD, readers are referred to, e.g., Refs. 9, 20, 60–62. We now describe the MMREMD method, whereby the REMD simulation can be performed with the arbitrary mass scaling with respect to temperatures and particles. Such mass scaling must be of great utility for application to biological systems, which have various masses from hydrogen to carbon, phos-

*Accepted on Oct. 31, 2016; Author's final version

[†]tnagai@nagoya-u.jp

phorus, and sulfur. This formalism would allow, for example, for changing active fluctuations according to respective temperatures.

We suppose a system consisting of N particles, whose coordinate and momentum vectors are defined by $q = \{q_1, \dots, q_N\}$ and $p = \{p_1, \dots, p_N\}$, respectively. The velocity vector is given by $\dot{q} = \{\dot{q}_1, \dots, \dot{q}_N\}$, where the dot represents the time derivative. Because the Hamiltonian is not necessarily identical among the temperatures,²²⁾ we set the mass of k th particle at T_ℓ to $m_{k,\ell} = \alpha_{k,\ell} m_k$, where $\alpha_{k,\ell}$ is the scaling factor of each mass. Thus the system at T_ℓ is described by $H_\ell = K_\ell(\dot{q}) + E(q)$, where the kinetic energy is given by $K_\ell = \sum_{k=1}^N \frac{\alpha_{k,\ell} m_k \dot{q}_k^2}{2}$, and E stands for the potential energy. The N_{rep} copies of the system (replicas) are simultaneously simulated at each temperature with the weight factor,

$$f_{\text{NVT}}(q, \dot{q}) \propto \exp[-K_\ell(\dot{q})/k_B T_\ell] \exp[-E(q)/k_B T_\ell], \quad (1)$$

at T_ℓ . The replica exchange can be attempted with the transition probability given by the standard Metropolis criterion,

$$\min[1, \exp(\Delta\beta\Delta E)], \quad (2)$$

where $\Delta\beta = 1/(k_B T_\ell) - 1/(k_B T_m)$ and $\Delta E = E_{i^{\text{old}}(\ell)} - E_{i^{\text{old}}(m)}$, with the generalized velocity scaling rules given by

$$\dot{q}_k^{[i^{\text{new}}(\ell)]'} = \sqrt{\frac{T_\ell}{T_m}} \sqrt{\frac{\alpha_{k,m}}{\alpha_{k,\ell}}} \dot{q}_k^{[i^{\text{new}}(\ell)]} = \sqrt{\frac{T_\ell}{T_m}} \sqrt{\frac{\alpha_{k,m}}{\alpha_{k,\ell}}} \dot{q}_k^{[i^{\text{old}}(m)]}, \quad (3)$$

$$\dot{q}_k^{[i^{\text{new}}(m)]'} = \sqrt{\frac{T_m}{T_\ell}} \sqrt{\frac{\alpha_{k,\ell}}{\alpha_{k,m}}} \dot{q}_k^{[i^{\text{new}}(m)]} = \sqrt{\frac{T_m}{T_\ell}} \sqrt{\frac{\alpha_{k,\ell}}{\alpha_{k,m}}} \dot{q}_k^{[i^{\text{old}}(\ell)]}. \quad (4)$$

Note that the superscripts of $i^{\text{old}}(\ell)$ and $i^{\text{new}}(\ell)$ represent the replica index coupling to T_ℓ before and after a replica-exchange attempt, respectively. It might be noteworthy that the momentum must obey the following different rules:

$$p_k^{[i^{\text{new}}(\ell)]'} = \sqrt{\frac{T_\ell}{T_m}} \sqrt{\frac{\alpha_{k,\ell}}{\alpha_{k,m}}} p_k^{[i^{\text{new}}(\ell)]} = \sqrt{\frac{T_\ell}{T_m}} \sqrt{\frac{\alpha_{k,\ell}}{\alpha_{k,m}}} p_k^{[i^{\text{old}}(m)]}, \quad (5)$$

$$p_k^{[i^{\text{new}}(m)]'} = \sqrt{\frac{T_m}{T_\ell}} \sqrt{\frac{\alpha_{k,m}}{\alpha_{k,\ell}}} p_k^{[i^{\text{new}}(m)]} = \sqrt{\frac{T_m}{T_\ell}} \sqrt{\frac{\alpha_{k,m}}{\alpha_{k,\ell}}} p_k^{[i^{\text{old}}(\ell)]}. \quad (6)$$

These scaling rules may be derived by imposing the cancellation of contributions from momenta or velocities to the detailed balance conditions. The derivation for a special case was detailed elsewhere.⁴³⁾

As MMREMD is the general formalism, the MSREMD method can be derived as a special case where $\alpha_{k,\ell}$ is set in proportion to T_ℓ , which yields the simplest velocity scaling rule:

$$\dot{q}_k^{[i^{\text{new}}(\ell)]'} = \dot{q}_k^{[i^{\text{new}}(\ell)]} = \dot{q}_k^{[i^{\text{old}}(m)]}, \quad (7)$$

$$\dot{q}_k^{[i^{\text{new}}(m)]'} = \dot{q}_k^{[i^{\text{new}}(m)]} = \dot{q}_k^{[i^{\text{old}}(\ell)]}. \quad (8)$$

Furthermore, it is apparent that the conventional velocity scaling rules for the original REMD method,

$$\dot{q}_k^{[i^{\text{new}}(\ell)]'} = \sqrt{\frac{T_\ell}{T_m}} \dot{q}_k^{[i^{\text{new}}(\ell)]} = \sqrt{\frac{T_\ell}{T_m}} \dot{q}_k^{[i^{\text{old}}(m)]}, \quad (9)$$

$$\dot{q}_k^{[i^{\text{new}}(m)]'} = \sqrt{\frac{T_m}{T_\ell}} \dot{q}_k^{[i^{\text{new}}(m)]} = \sqrt{\frac{T_m}{T_\ell}} \dot{q}_k^{[i^{\text{old}}(\ell)]}, \quad (10)$$

may be deduced as a special case for which $\alpha_{k,\ell} = 1$.

The above formalism is sufficient for the Langevin⁶³⁾ and Andersen⁶⁴⁾ thermostats. Nevertheless, when the Nosé–Hoover thermostat^{65,66)} is employed for the canonical simulation, an additional treatment is necessary owing to an extra term of the Nosé–Hoover thermostat. The treatment is detailed in Refs. 62 and 42.

To summarize, the MMREMD simulations can be performed as follows: (1) prepare N_{rep} replicas with mass m_k multiplied by an arbitrary factor of $\alpha_{k,\ell}$ at T_ℓ ; (2) perform the N_{rep} independent canonical MD simulations at each temperature; (3) exchange the replicas according to the probability given by Eq. (2) with the generalized rules given by Eqs. (3) and (4) [for momentum, Eqs. (5) and (6)]; (4) repeat steps (2)–(3) until the simulation ends.

2.2 Review and refinement of V-REMD

Reviewing the V-REMD method,⁵¹⁾ we now give its improvement based on the general formalism. Similarly to the original REMD method, the V-REMD method involves N_{rep} noninteracting replicas simulated at N_{rep} different temperatures. The V-REMD method manipulates the solvent viscosity by scaling masses depending on temperature. The change in the mass of water by the factor α changes the viscosity of the factor $\sqrt{\alpha}$.^{51,67,68)} The reduced solvent viscosity provides faster kinetics and thus expedites the MD simulations.^{49,69–77)} In Ref. 51, the original mass values were used at one temperature to study biologically relevant properties, whereas the reduced mass values (0.2 times as large as the original values, i.e., $\alpha_{k,\ell} = 0.2$) were used with respect to the atoms of water molecules at the other temperatures. The conventional momentum scaling rules²⁰⁾ were employed [for the corresponding velocity scaling rules, see Eqs. (9) and (10)]. Nevertheless, in order to satisfy the detailed balance condition, we should adhere to Eqs. (3)–(6), which are used in the new version of the V-REMD method. Hereafter, we refer to the original version as V-REMD-1 (or ‘V-1’ for short in figure legends) and to the refined version with Eqs. (3)–(6) as V-REMD-2 (or ‘V-2’).

2.3 Models

We employed a Lennard-Jones (LJ) fluid as a useful pilot system. The potential energy is given by

$$E = \sum_{i<j} V_{ij}, \quad (11)$$

$$V_{ij} = 4\epsilon \left[\left(\frac{\sigma}{r_{ij}} \right)^{12} - \left(\frac{\sigma}{r_{ij}} \right)^6 \right], \quad (12)$$

where ϵ and σ represent the value of the potential minimum and the diameter of particles, respectively, and r_{ij} the distance between the i th and j th particles. In what follows, we use reduced units; we set $\sigma = 1$, $\epsilon = 1$, and $k_B = 1$.

2.4 Numerical details for Nosé–Hoover thermostats

As for the Nosé–Hoover dynamics, an in-house program was used with the time-reversible integrator⁷⁸⁾ using the Suzuki–Trotter decomposition corresponding to Integrator 1 in Ref. 79. For a pseudorandom number generator, the

Mersenne twister⁸⁰⁾ was employed.

We performed the original⁵¹⁾ (V-REMD-1) and refined (V-REMD-2) versions of the V-REMD simulations. In accordance with Ref. 51 the particle mass was set to unity at the lowest temperature T_1 ($\alpha_{k,1} = 1$), and at other temperatures the mass was set to 0.2 ($\alpha_{k,\ell} = 0.2$ for $\ell \neq 1$). Although this is a special case of V-REMD where there is no solute in the system, it must be sufficient for the validation and evaluation of the new approach, as the change in the algorithm between the two versions is limited to the treatment of solvent molecules.

The mass of the thermostat was set in proportion to temperatures. Those at the lowest temperature T_1 were set to $Q_0 = 1, 10, \text{ and } 1000$. These values are fine, but the value of 0.1 was unreasonable even for the conventional canonical simulations. In general, very small values for Q do not guarantee the equilibrium due to the isolated mode of a heat bath.⁸¹⁾ With g being the degree of freedom, the typical oscillation period with the thermostat is given by $\tau_{\text{NH}} \sim 2\pi \sqrt{\frac{Q}{2gk_{\text{B}}T}}$,⁸¹⁾ corresponding to $\tau_{\text{NH}} \sim 0.16, 0.51, \text{ and } 5.1$ for $Q_0 = 1, 10, \text{ and } 1000$, respectively.

The replica exchange was attempted every single MD step ($N_{\text{ex}} = 1$) as regards V-REMD-2 simulations. These frequent attempts are based on Refs. 57–59 for the optimally enhanced efficiency.⁸²⁾ In regard to the V-REMD-1, the replica exchange was attempted every $N_{\text{ex}} = 5, 100, \text{ and } 1000$ MD steps. Even though the frequent replica-exchange attempts are encouraged,^{57–59)} it was not feasible for the V-REMD-1 method to use $N_{\text{ex}} = 1$ owing to numerical divergence.

The time step of 0.005 was employed and each simulation lasted for 4×10^5 steps, corresponding to 2000 unit time. The number of replicas was eight ($N_{\text{rep}} = 8$) and the reference temperatures were 1.000, 1.104, 1.219, 1.346, 1.486, 1.641, 1.812, and 2.000. These temperatures are referred to as T_1 to T_8 . The replica-exchange acceptance ratios ranged from 13 to 19 % in all V-REMD-2 simulations, in agreement with those of the REMD simulations.⁴²⁾ Five hundred identical LJ particles were placed ($N = 500$) in a cube of sides 8.55 in the reduced unit length, corresponding to a number density of $\rho = 0.800$. In these thermal conditions, the LJ fluid is in the liquid phase.⁸³⁾ The periodic boundary condition was employed. After the MD step of nN_{ex} ($n = 1, 2, 3 \dots$), the replica-exchange attempts were made in turn. The LJ forces were just truncated at 3 ($r_c = 3$) in the reduced unit; accordingly, the LJ potential was shifted upward by $|V_{ij}(r_c)|$ for $r_{ij} < r_c$.

2.5 Numerical details for Langevin dynamics

In order to further investigate the utility of the present formalism, the Langevin thermostat was examined with almost the same conditions. The characteristic parameter of the thermostat is not the mass but the friction coefficient γ and the inverse gives the time constant. The integrator implemented on the basis of Ref. 84 reads

$$\dot{q} \leftarrow e^{-\gamma\Delta t} \dot{q} + \sqrt{\frac{k_{\text{B}}T}{m}} \sqrt{(1 - e^{-\gamma\Delta t})(1 + e^{-\gamma\Delta t})} R, \quad (13)$$

$$\dot{q} \leftarrow \dot{q} + \frac{f}{m} \frac{\Delta t}{2}, \quad (14)$$

$$q \leftarrow q + \dot{q}\Delta t, \quad (15)$$

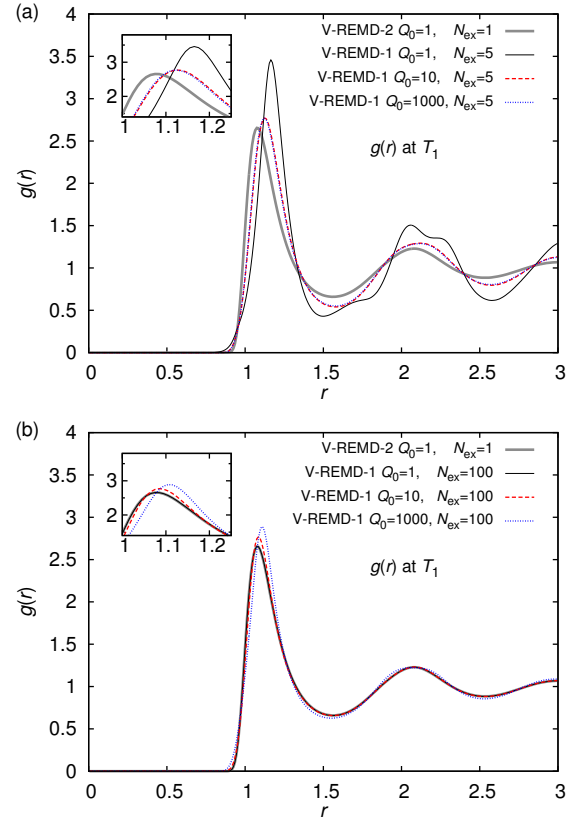


Fig. 1. (Color online) Radial distribution functions $g(r)$ at T_1 are plotted for V-REMD-1 with (a) $N_{\text{ex}} = 5$ and (b) $N_{\text{ex}} = 100$ together with one obtained with V-REMD-2 with $Q_0 = 1$ and $N_{\text{ex}} = 1$ (gray thick line). The black thin, red dashed, and blue dotted lines mark V-REMD-1 with $Q_0 = 1, 10, \text{ and } 1000$, respectively.

$$\dot{q} \leftarrow \dot{q} + \frac{f}{m} \frac{\Delta t}{2}, \quad (16)$$

where f stands for the force and R is a random number drawn from the normalized Gaussian distribution. This integrator allows for arbitrary values for γ in contrast to some Langevin dynamics integrators demanding $\gamma\Delta t \ll 1$. For $\gamma \rightarrow \infty$, all the velocities are drawn from the Maxwell-Boltzmann distribution every single update described in Eq. (13). Thus, any artifact in velocity can be removed every single MD step. Nevertheless, very large γ values are not optimal for the efficiency of simulations. For example, Ref. 76 reports the mean first passage time of transitions with γ from 0.5 to 50 ps^{-1} , showing that the smaller γ is better within the range regarding the alanine dipeptide simulation. In fact, both the very small and very large γ values were shown to be inefficient.⁸⁴⁾ Here, the values of γ were set to 1, 10, and 100, with the coupling times corresponding to 1, 0.1, and 0.01, respectively. The γ values of 100 does not satisfy $\gamma\Delta t \ll 1$. The replica-exchange attempts were performed at an interval of $N_{\text{ex}} = 1$ and 100 MD steps in the V-REMD-1 simulations. As regards the V-REMD-2 simulations, the interval was set to $N_{\text{ex}} = 1$. The Gaussian random number was generated by the Box-Muller method⁸⁵⁾ with uniform pseudo-random numbers obtained with the Mersenne twister.⁸⁰⁾

3. Results and Discussion

With frequent replica-exchange attempts, a large discrepancy in the radial distribution function between the V-REMD-

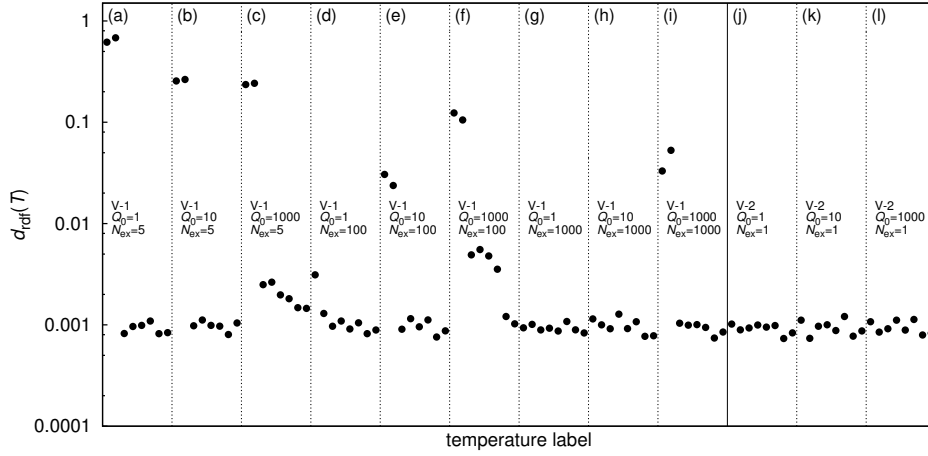


Fig. 2. The difference in the radial distribution function $g(r)$ between the present simulations and the previous REMD simulation,⁴²⁾ defined by $\int |g(r) - g_{\text{REMD}}(r)| dr$, is plotted. Each panel contains 8 points corresponding to T_1 to T_8 from left to right. Panels (a), (b), and (c) show V-REMD-1 with $N_{\text{ex}} = 5$ with $Q_0 = 1, 10,$ and $1000,$ respectively. Similarly, panels (d), (e), and (f) show V-REMD-1 with $N_{\text{ex}} = 100$ with $Q_0 = 1, 10,$ and $1000,$ and panels (g), (h), and (i) show V-REMD-1 with $N_{\text{ex}} = 1000$ with $Q_0 = 1, 10,$ and $1000,$ respectively. Panels (j), (k), and (l) show V-REMD-2 with $N_{\text{ex}} = 1$ with $Q_0 = 1, 10,$ and $1000,$ respectively. The values of parameters are also given in the panel.

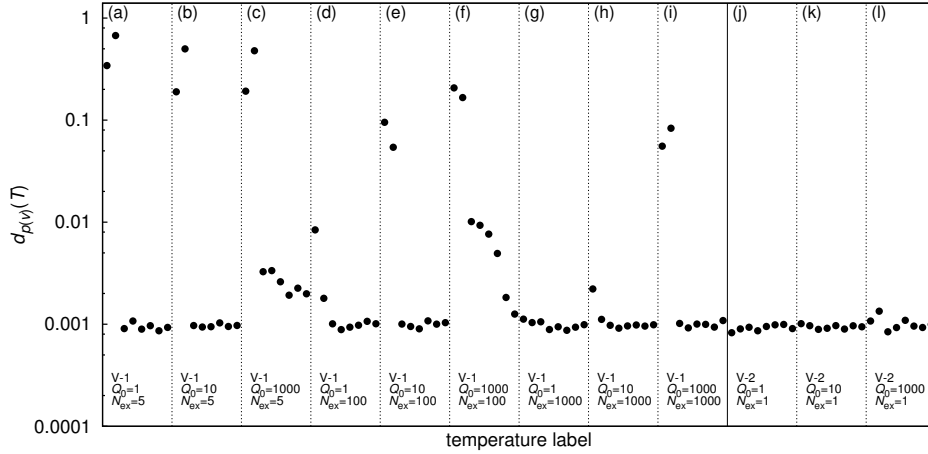


Fig. 3. Plotted is the difference between the theoretical curve and results of simulations, as measured by $d_p \equiv \int |p_{\text{simulation}}(v) - p_B(v)| dv$. Each panel contains 8 points corresponding to T_1 to T_8 from left to right. Panels (a) to (i) are obtained with the V-REMD-1 method, and panels (j) to (l) with V-REMD-2. Panels (a), (b), and (c) show V-REMD-1 with $N_{\text{ex}} = 5$ with $Q_0 = 1, 10,$ and $1000,$ respectively. Similarly, panels (d), (e), and (f) show V-REMD-1 with $N_{\text{ex}} = 100$ with $Q_0 = 1, 10,$ and $1000,$ and panels (g), (h), and (i) show V-REMD-1 with $N_{\text{ex}} = 1000$ with $Q_0 = 1, 10,$ and $1000,$ respectively. Panels (j), (k), and (l) show V-REMD-2 with $N_{\text{ex}} = 1$ with $Q_0 = 1, 10,$ and $1000,$ respectively. The values of parameters are also given in the panel, in which V-1 and V-2 stand for V-REMD-1 and V-REMD-2, respectively.

1 and V-REMD-2 simulations was observed [Figure 1(a)], in the application with the Nosé–Hoover thermostat. In particular, the radial distribution function $g(r)$ of the V-REMD-1 with $Q_0 = 1$ and $N_{\text{ex}} = 5$ exhibits unusual peaks (at $r \approx 1.7$ and 2.3), thus losing even qualitative agreement. Even for $N_{\text{ex}} = 100$ [see Fig. 1(b)], some discrepancy persists. The deviation from a straight REMD simulation⁴²⁾ at each temperature is shown in Fig. 2, as measured by

$$d_{\text{rdf}} = \int_0^{r_c(=3)} |g(r) - g_{\text{REMD}}(r)| dr. \quad (17)$$

Whereas the V-REMD-2 simulations agree with the conventional REMD simulation, the V-REMD-1 simulations exhibit apparent disagreements, except for $N_{\text{ex}} = 1000$ with $Q_0 = 1$ or 10 . As the disagreements are profound particularly at the two lowest temperatures, where the wrong scaling rules are

employed, they should be thought of as an artifact and be ascribed to the inappropriate velocity scaling in V-REMD-1. As such artifacts in the solvent structures should spoil the correct solvation of biomolecules, the appropriate velocity scaling rules are crucial to performing reliable V-REMD simulations.

In the probability density of velocity, an apparent discrepancy from the Boltzmann distribution $p_B(v) = \frac{1}{\sqrt{2\pi T/m}} \exp\left[-\frac{mv^2}{2T}\right]$ was observed in the V-REMD-1 simulations, whereas the V-REMD-2 simulations were free from such a deviation. This discrepancy was illustrated in Fig. 3, evaluated using

$$d_p \equiv \int |p_{\text{simulation}}(v) - p_B(v)| dv \quad (18)$$

at each temperature for all simulations. Even though the de-

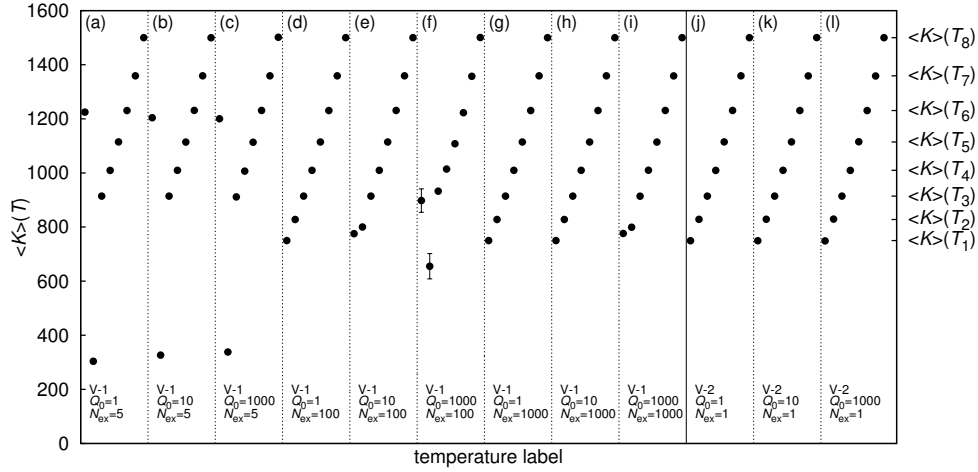


Fig. 4. Average kinetic energy $\langle K_\ell \rangle$ is plotted. The theoretical averages $\frac{3}{2}Nk_B T$ are indicated on the right vertical axis. Each panel contains 8 points corresponding to T_1 to T_8 from left to right. Bars show the error estimated with the jackknife method^{61,86,87}. Panels (a), (b), and (c) show V-REMD-1 with $N_{\text{ex}} = 5$ with $Q_0 = 1, 10,$ and $1000,$ respectively. Similarly, panels (d), (e), and (f) show V-REMD-1 with $N_{\text{ex}} = 100$ with $Q_0 = 1, 10,$ and $1000,$ and panels (g), (h), and (i) show V-REMD-1 with $N_{\text{ex}} = 1000$ with $Q_0 = 1, 10,$ and $1000,$ respectively. Panels (j), (k), and (l) show V-REMD-2 with $N_{\text{ex}} = 1$ with $Q_0 = 1, 10,$ and $1000,$ respectively.

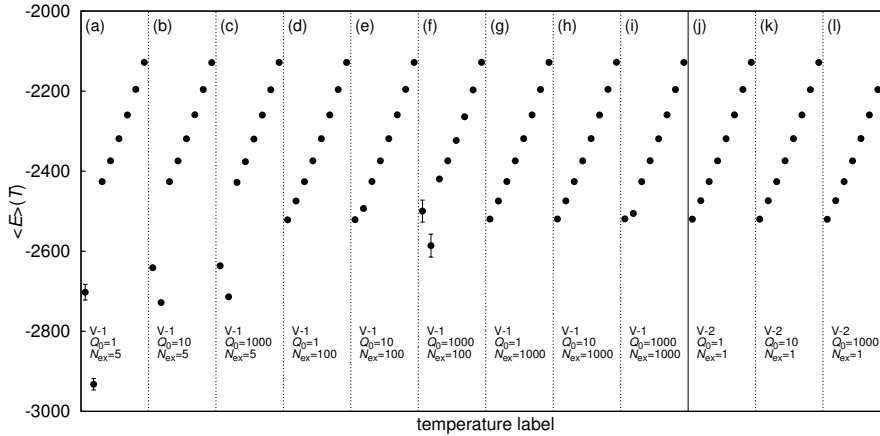


Fig. 5. Average potential energy $\langle E \rangle$ is plotted. Each panel contains 8 points corresponding to T_1 to T_8 from left to right. Bars show the error estimated with the jackknife method^{61,86,87}. Panels (a), (b), and (c) show V-REMD-1 with $N_{\text{ex}} = 5$ with $Q_0 = 1, 10,$ and $1000,$ respectively. Similarly, panels (d), (e), and (f) show V-REMD-1 with $N_{\text{ex}} = 100$ with $Q_0 = 1, 10,$ and $1000,$ and panels (g), (h), and (i) show V-REMD-1 with $N_{\text{ex}} = 1000$ with $Q_0 = 1, 10,$ and $1000,$ respectively. Panels (j), (k), and (l) show V-REMD-2 with $N_{\text{ex}} = 1$ with $Q_0 = 1, 10,$ and $1000,$ respectively. The values of parameters are also given in the panel.

viation is softened by less frequent exchange attempts, it may persist throughout the acceptable parameters of Q_0 . The discrepancy is more notable especially at the two lowest temperatures with more frequent exchange attempts in V-REMD-1 simulations. On the other hand, the V-REMD-2 simulations are fine with the very frequent exchange attempt over a wide range of values for Q_0 .

Figure 4 shows the average kinetic energy $\langle K_\ell \rangle = \left\langle \sum_{k=1}^N \frac{a_{k,\ell} m_k \dot{q}_{k,\ell}^2}{2} \right\rangle$. In accordance with the observation on d_p , the temperature is not correctly controlled in most of the V-REMD-1 simulations, as indicated by the shift of the average kinetic energy. Whereas the less frequent replica-exchange attempts make the shift less profound, the V-REMD-2 simulations work perfectly with the frequent exchange attempts ensuring the enhanced efficiency according to Refs. 57–59. The errors were obtained by the jackknife method^{61,86,87} with twenty bins. Accordingly, a marked discrepancy was observed

in the average potential energy between most of the V-REMD-1 simulations especially at the two lowest temperatures (see Fig. 5), suggesting the unreliability of the conventional version. In contrast, the agreement is found between V-REMD-2 simulations, indicating the soundness of this new version. These results clearly demonstrate the importance of the adherence to the correct scaling rule in accordance with the mass scaling.

Even though the artifacts mentioned above are minor in the V-REMD-1 simulation with the particular parameter values of $Q_0 = 1$ and $N_{\text{ex}} = 1000$, this is not the case for heat capacity, as illustrated in Fig. 6. The heat capacity at T_ℓ was obtained through the fluctuation of the total energy, $C = \left(\langle H_\ell^2 \rangle - \langle H_\ell \rangle^2 \right) / T_\ell^2$. The errors were obtained using the jackknife method^{61,86,87} with twenty bins. The deviation in heat capacity suggests that the correct energetics between solute and solvent, which should be of importance for the cor-

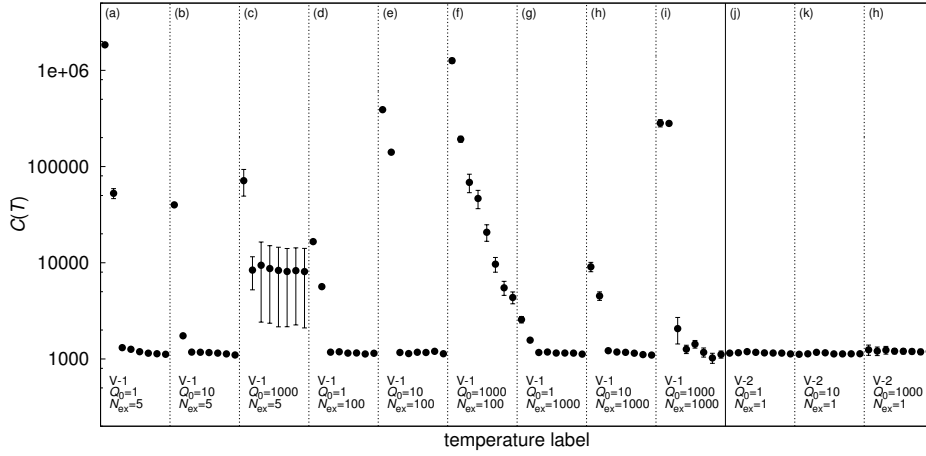


Fig. 6. Heat capacity C is plotted. Each panel contains 8 points corresponding to T_1 to T_8 from left to right. Bars show the error estimated with the jackknife method^{61,86,87}. Panels (a), (b), and (c) show V-REMD-1 with $N_{\text{ex}} = 5$ with $Q_0 = 1, 10$, and 1000 , respectively. Similarly, panels (d), (e), and (f) show V-REMD-1 with $N_{\text{ex}} = 100$ with $Q_0 = 1, 10$, and 1000 , and panels (g), (h), and (i) show V-REMD-1 with $N_{\text{ex}} = 1000$ with $Q_0 = 1, 10$, and 1000 , respectively. Panels (j), (k), and (l) show V-REMD-2 with $N_{\text{ex}} = 1$ with $Q_0 = 1, 10$, and 1000 , respectively.

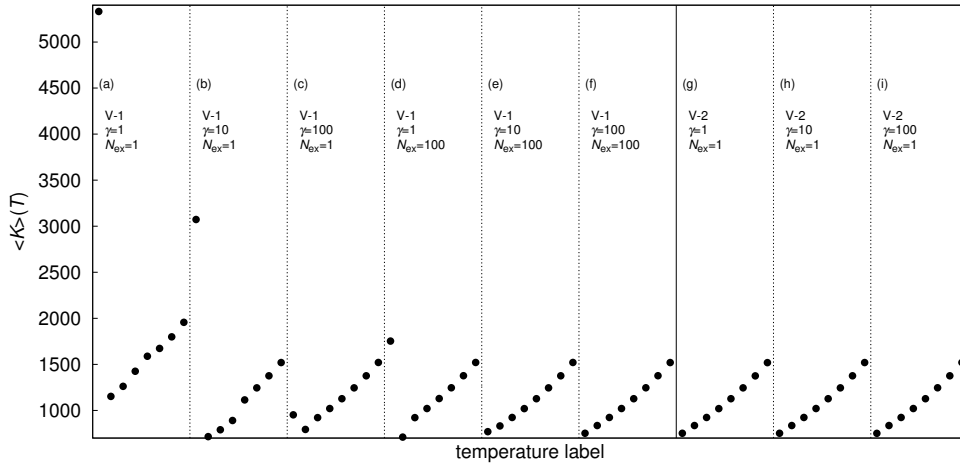


Fig. 7. Average kinetic energy $\langle K \rangle$ obtained with the Langevin thermostat is plotted. Not exceeding the size of marks, error bars estimated with the jackknife method^{61,86,87} are invisible. Panels (a), (b), and (c) show V-REMD-1 with $N_{\text{ex}} = 1$ with $\gamma = 1, 10$, and 100 , respectively. Similarly, panels (d), (e), and (f) show V-REMD-1 with $N_{\text{ex}} = 100$ with $\gamma = 1, 10$, and 100 , and panels (g), (h), and (i) show V-REMD-2 with $N_{\text{ex}} = 1$ with $\gamma = 1, 10$, and 100 , respectively.

rect enhanced sampling, can be destroyed by the inappropriate algorithm. Furthermore, this result implies that the distortion introduced to some physical quantities by the inappropriate velocity scaling may persist in a wide range of setups. On the other hand, the V-REMD-2 method does not introduce any artifact even with the frequent replica-exchange attempts required for optimal performance,^{57–59} establishing the indispensability of the new formalism.

As an artifact of V-REMD-1 with $N_{\text{ex}} = 5$, large potential energy gaps were introduced between T_2 and T_3 (Figure 5), which hinder the replica exchanges. As few exchanges are accepted, the thermodynamic averages were more or less correct above T_3 . The persistent artifact in heat capacity found for $Q_0 = 1000$ and $N_{\text{ex}} = 5$ up to the highest temperature arose from the slow convergence of the artifact introduced at the early stage of the simulation. With regard to the condition of $Q_0 = 1000$ with $N_{\text{ex}} = 100$, the acceptance ratio between T_2 and T_3 was as high as 37 %, presumably owing to the large energy fluctuation reflected on the large error bars.

Thus, the artifact generated by the inappropriate velocity scaling between T_1 and T_2 was recurrently introduced to the upper temperatures.

In the application with Langevin dynamics, the universality of the above discussion was examined. Figures 7 and 8 show the average kinetic and potential energy functions, respectively. With the small γ and the small N_{ex} , the apparent discrepancy was found, similarly to the Nosé–Hoover case. Moreover, heat capacity was affected by the wrong velocity scaling of V-REMD-1 in a wide range of parameters (Figure 9). In fact, no significant deviation was found even in the heat capacity for the large γ of 20000 with $N_{\text{ex}} = 1$, although the errors tended to be larger than those of the V-REMD-2 simulations with $\gamma = 1, 10$, and 100 . However, this must not be the case if the integrator is rearranged so that Eq. (13) is performed after Eq. (16) (but before the replica-exchange attempts). On the other hand, the V-REMD-2 method demonstrates its rigorosity permitting the frequent exchange and small friction coefficient.

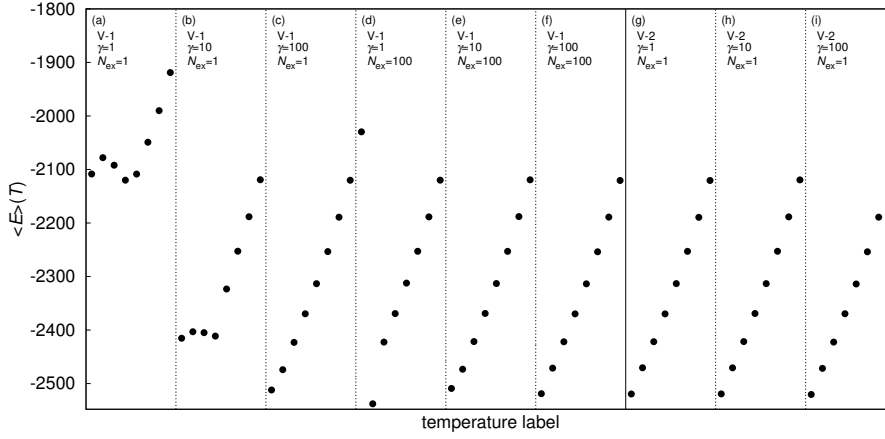


Fig. 8. Average potential energy $\langle E \rangle$ obtained with the Langevin thermostat is plotted. Each panel contains 8 points corresponding to T_1 to T_8 from left to right. Not exceeding the size of marks, error bars estimated with the jackknife method^{61,86,87}) are invisible. Panels (a), (b), and (c) show V-REMD-1 with $N_{\text{ex}} = 1$ with $\gamma = 1, 10$, and 100 , respectively. Similarly, panels (d), (e), and (f) show V-REMD-1 with $N_{\text{ex}} = 100$ with $\gamma = 1, 10$, and 100 , and panels (g), (h), and (i) show V-REMD-2 with $N_{\text{ex}} = 1$ with $\gamma = 1, 10$, and 100 , respectively. The values of parameters are also given in the panel.

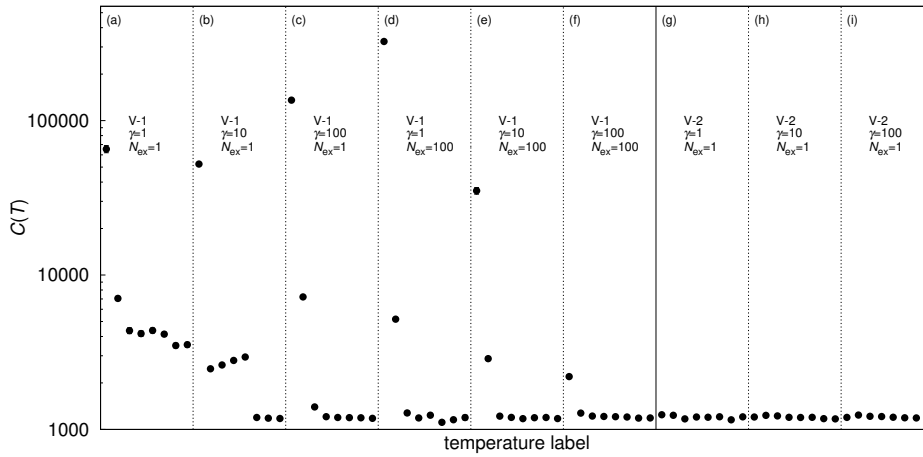


Fig. 9. Heat capacity C obtained with the Langevin thermostat is plotted. Each panel contains 8 points corresponding to T_1 to T_8 from left to right. Not exceeding the size of marks, error bars estimated with the jackknife method^{61,86,87}) are almost invisible. Panels (a), (b), and (c) show V-REMD-1 with $N_{\text{ex}} = 1$ with $\gamma = 1, 10$, and 100 , respectively. Similarly, panels (d), (e), and (f) show V-REMD-1 with $N_{\text{ex}} = 100$ with $\gamma = 1, 10$, and 100 , respectively, and panels (g), (h), and (i) show V-REMD-2 with $N_{\text{ex}} = 1$ with $\gamma = 1, 10$, and 100 , respectively.

It is noticeable that the deviation behavior is different between the two thermostats. For example, the lowered kinetic energy at T_2 found in the application with the Nosé–Hoover thermostat (see Fig. 4) is hardly observed with the Langevin dynamics (see Fig. 7). The difference should be attributed to the difference in the dynamics related to the thermostats. In particular, on the way to thermalization, the Nosé–Hoover thermostat involves fluctuations in temperature, while the Langevin dynamics exhibits exponential decay.⁸⁸) It may be noteworthy that, as long as V-REMD-2 is employed, no profound artifacts were found regardless of the thermostats used even with the very frequent replica-exchange attempts. Therefore, any thermostats generating the canonical distributions should be applicable to REMD with frequent replica-exchange attempts. Nevertheless, some particular cautions are necessary depending on the thermostat. For example, the Nosé–Hoover thermostat should request well-thermalized initial conditions because of the slow and fluctuating equilibration.

We demonstrate that the results of V-REMD-1 simulations can be notably erroneous owing to the incorrect velocity scaling rules that do not take mass scaling into account. Whereas the artifacts are attributable to the incorrect algorithm; they can be milder when Q_0 is smaller and N_{ex} is larger. For a larger value of N_{ex} , the artifacts are introduced less frequently. Presumably, the faster relaxation of the thermostat owing to a smaller Q_0 eases the artifacts introduced by the incorrect velocity scaling. Correspondingly, the larger values of γ and the larger values of N_{ex} ease the artifact in the V-REMD-1 simulation with the Langevin thermostat, while the V-REMD-2 method can employ small values of γ and N_{ex} . The (moderately) small γ and small N_{ex} are important for efficiency. Therefore the current formalism is indispensable for various implementations of V-REMD involving different thermostats.

Optimistically, with a much shorter relaxation time of the thermostat than the replica-exchange attempt interval, practically acceptable results may be obtained even with V-REMD-1. Note that in Ref. 51, the replica exchange was attempted at

an interval of 1.5 ps (750 MD steps) and that the Berendsen thermostat⁸⁹⁾ was used with the coupling time of 0.1 ps, seemingly satisfying the above considerations. Generally, the employment of the Berendsen thermostat with REMD is risky⁵⁹⁾ as the distribution is not a canonical one⁹⁰⁾ for finite values for the coupling time of a heat bath, despite the assumption of the canonical distribution in the replica-exchange algorithm. Only for the mathematically achievable limit where the coupling time tends to zero, the canonical distribution of configuration can be obtained.⁹¹⁾ Nevertheless, as far as Ref. 92 claims, if the interval of replica-exchange attempts is much larger than the coupling time, an artifact⁹³⁾ introduced owing to the employment of the Berendsen thermostat to REMD is not profound. Therefore the artifact of the Berendsen thermostat may not be significant in Ref. 51. It is possible that the V-REMD method has demonstrated its efficiency with a sub-optimal yet fortunate combination of parameters, with which artifacts are slim. Nevertheless, the large values of Q_0 with the Nosé–Hoover thermostat are acceptable for the correct canonical simulations, and small numbers for N_{ex} are actually recommended for the optimal REMD simulations.^{57–59)} In addition, the moderately small friction coefficient is advocated for the optimal sampling via Langevin dynamics. In fact, some Langevin dynamics integrators assume a small value of γ . Therefore the general formalism is crucial for easier and more optimized applicability of the promising V-REMD method.

4. Conclusions

We formalized the general mass scaling approach to the REMD method, which is particularly referred to as the MM-REMD method. With the general formalism, arbitrary mass scaling can be combined with the REMD simulations, which will be of great utility in applications to biological systems. As both the mass scaling and REMD have shown their great utility, the combination must be promising. One preceding special case was the MSREMD method, in which all the masses were scaled in proportion to temperature to stabilize the simulations.⁴²⁾ In this work, as a new concrete application of the general formalism, we reviewed the V-REMD method,⁵¹⁾ which utilizes light solvent molecules at high temperatures, thereby decreasing viscosity to enhance the sampling efficiency. We proposed the refined version of the V-REMD method, which is referred to as V-REMD-2 above, via the general formalism. We applied the original and refined versions of V-REMD to a pilot system of the Lennard-Jones fluid to validate and evaluate the novel formalism. We demonstrated that the new velocity scaling rules obtained with the novel formalism are crucial for the accurate Boltzmann sampling, especially when frequent replica-exchange attempts are made as per Refs. 57–59. The radial distribution functions are distorted by the incorrect scaling. Thus this wrong solvent structure would in turn harm the correctness of solute structures. Heat capacity deviates owing to the improper scaling over a wide range of parameters, which would distort the energetics between solute and solvent in future advanced applications. On the other hand, the new version of V-REMD (V-REMD-2) is free from such artifacts. By eliminating the necessity of a particular parameter setting and less frequent replica-exchange attempts that are not optimal,^{57–59)} the novel formalism makes the V-REMD method more sound and of better availability. In conclusion, we formalized the mass-

scaling approach in REMD and established the importance of correct velocity scaling rules, whereby more rigorous and efficient simulations will be performed.

Acknowledgments

Some of the computations were performed at the Research Center for Computational Science, Okazaki, Japan. This work was, in part, supported by a Grant-in-Aid for Young Scientists (B) under Grant No. 26790083. The author thanks Dr. Takahashi of Ritsumeikan University for helpful discussion.

- 1) U. H. E. Hansmann and Y. Okamoto, in *Annual Reviews of Computational Physics VI*, ed. D. Stauffer, World Scientific, Singapore, 1999, p. 129.
- 2) A. Mitsutake, Y. Sugita, and Y. Okamoto, *Biopolymers* **60**, 96 (2001).
- 3) Y. Sugita and Y. Okamoto, in *Lecture Notes in Computational Science and Engineering*, eds. T. Schlick and H. H. Gan, Springer, Heidelberg, 2002, p. 304; <http://arxiv.org/abs/cond-mat/0102296>.
- 4) A. Morriss-Andrews and J.-E. Shea, *Annu. Rev. Phys. Chem.* **66**, 643 (2015).
- 5) B. A. Berg and T. Neuhaus, *Phys. Lett. B* **267**, 249 (1991).
- 6) B. A. Berg and T. Neuhaus, *Phys. Rev. Lett.* **68**, 9 (1992).
- 7) A. P. Lyubartsev, A. A. Martsinovski, S. V. Shevkunov, and P. N. Vorontsov-Velyaminov, *J. Chem. Phys.* **96**, 1776 (1992).
- 8) E. Marinari and G. Parisi, *Europhys. Lett.* **19**, 451 (1992).
- 9) K. Hukushima and K. Nemoto, *J. Phys. Soc. Jpn.* **65**, 1604 (1996).
- 10) C. J. Geyer, in *Computing Science and Statistics, Proceedings of the 23rd Symposium on the Interface*, ed. E. M. Keramidas, Interface Foundation of North America, Fairfax Station, VA, 1991 p. 156.
- 11) F. Wang and D. P. Landau, *Phys. Rev. Lett.* **86**, 2050 (2001).
- 12) F. Wang and D. P. Landau, *Phys. Rev. E* **64**, 056101 (2001).
- 13) J. Kim, J. E. Straub, and T. Keyes, *J. Chem. Phys.* **126**, 135101 (2007).
- 14) J. Kim, T. Keyes, and J. E. Straub, *J. Chem. Phys.* **130**, 124112 (2009).
- 15) J. Kim, J. E. Straub, and T. Keyes, *J. Phys. Chem. B* **116**, 8646 (2012).
- 16) A. Laio and M. Parrinello, *Proc. Natl. Acad. Sci. U.S.A.* **99**, 12562 (2002).
- 17) T. Morishita, S. G. Itoh, H. Okumura, and M. Mikami, *Phys. Rev. E* **85**, 021201 (2012).
- 18) R. H. Swendsen and J.-S. Wang, *Phys. Rev. Lett.* **57**, 2607 (1986).
- 19) J.-S. Wang and R. H. Swendsen, *Prog. Theor. Phys. Supp.* **157**, 317 (2005).
- 20) Y. Sugita and Y. Okamoto, *Chem. Phys. Lett.* **314**, 141 (1999).
- 21) T. Nagai, R. Ueoka, and Y. Okamoto, *J. Phys. Soc. Jpn.* **81**, 024002 (2012).
- 22) Y. Sugita, A. Kitao, and Y. Okamoto, *J. Chem. Phys.* **113**, 6042 (2000).
- 23) A. Mitsutake and Y. Okamoto, *Phys. Rev. E* **79**, 047701 (2009).
- 24) A. Mitsutake and Y. Okamoto, *J. Chem. Phys.* **130**, 214105 (2009).
- 25) A. Mitsutake, *J. Chem. Phys.* **131**, 094105 (2009).
- 26) T. Nagai and Y. Okamoto, *Phys. Rev. E* **86**, 056705 (2012).
- 27) T. Nagai, Y. Okamoto, and W. Janke, *J. Stat. Mech. Theory E* **2013**, P02039 (2013).
- 28) T. Nishikawa, H. Ohtsuka, Y. Sugita, M. Mikami, and Y. Okamoto, *Prog. Theor. Phys. Supp.* **138**, 270 (2000).
- 29) T. Okabe, M. Kawata, Y. Okamoto, and M. Mikami, *Chem. Phys. Lett.* **335**, 435 (2001).
- 30) D. Paschek and A. García, *Phys. Rev. Lett.* **93**, 10 (2004).
- 31) Y. Mori and Y. Okamoto, *J. Phys. Soc. Jpn.* **79**, 074003 (2010).
- 32) C. Tsallis, *J. Stat. Phys.* **52**, 479 (1988).
- 33) J. Kim, T. Keyes, and J. E. Straub, *J. Chem. Phys.* **132**, 224107 (2010).
- 34) J. D. Chodera and M. R. Shirts, *J. Chem. Phys.* **135**, 194110 (2011).
- 35) S. G. Itoh and H. Okumura, *J. Chem. Theory Comput.* **9**, 570 (2013).
- 36) E. Lyman, F. M. Ytreberg, and D. M. Zuckerman, *Phys. Rev. Lett.* **96**, 028105 (2006).
- 37) K. Moritsugu, T. Terada, and A. Kidera, *J. Chem. Phys.* **133**, 224105 (2010).
- 38) Y. Yamamori and A. Kitao, *J. Chem. Phys.* **139**, 145105 (2013).
- 39) P. Liu, B. Kim, R. A. Friesner, and B. J. Berne, *Proc. Natl. Acad. Sci. U.S.A.* **102**, 13749 (2005).
- 40) T. Terakawa, T. Kameda, and S. Takada, *J. Comput. Chem.* **32**, 1228 (2011).

- (2011).
- 41) S. L. C. Moors, S. Michielssens, and A. Ceulemans, *J. Chem. Theory Comput.* **7**, 231 (2011).
 - 42) T. Nagai and T. Takahashi, *J. Chem. Phys.* **141**, 114111 (2014).
 - 43) T. Nagai and T. Takahashi, *JPS Conf. Proc.* **5**, 011009 (2015).
 - 44) C. H. Bennett, *J. Comput. Phys.* **19**, 267 (1975).
 - 45) R. Pomès and J. McCammon, *Chem. Phys. Lett.* **166**, 425 (1990).
 - 46) B. Mao, *Biophys. J.* **60**, 611 (1991).
 - 47) B. Mao, G. M. Maggiora, and K. C. Chou, *Biopolymers* **31**, 1077 (1991).
 - 48) K. A. Feenstra, B. Hess, and H. J. C. Berendsen, *J. Comput. Chem.* **20**, 786 (1999).
 - 49) R. Walser and W. F. van Gunsteren, *Proteins* **42**, 414 (2001).
 - 50) H. Zheng, S. Wang, and Y. Zhang, *J. Comput. Chem.* **30**, 2706 (2009).
 - 51) P. H. Nguyen, *J. Chem. Phys.* **132**, 144109 (2010).
 - 52) I.-C. Lin and M. E. Tuckerman, *J. Phys. Chem. B* **114**, 15935 (2010).
 - 53) E. Tsuchida, *J. Chem. Phys.* **134**, 044112 (2011).
 - 54) C. W. Hopkins, S. Le Grand, R. C. Walker, and A. E. Roitberg, *J. Chem. Theory Comput.* **11**, 1864 (2015).
 - 55) Y. P. Pang, *Biochem. and Biophys. Reports* **4**, 126 (2015).
 - 56) T. Nagai, G. A. Pantelopulos, T. Takahashi, and J. E. Straub, *J. Comput. Chem.* **37**, 2017 (2016).
 - 57) D. J. Sindhikara, Y. Meng, and A. E. Roitberg, *J. Chem. Phys.* **128**, 024103 (2008).
 - 58) D. J. Sindhikara, D. J. Emerson, and A. E. Roitberg, *J. Chem. Theory Comput.* **6**, 2804 (2010).
 - 59) E. Rosta and G. Hummer, *J. Chem. Phys.* **131**, 165102 (2009).
 - 60) D. Frenkel and B. Smit, *Understanding Molecular Simulation: From Algorithms to Applications* (Elsevier, San Diego, 2001).
 - 61) B. A. Berg, *Markov Chain Monte Carlo Simulations and Their Statistical Analysis* (World Scientific, Singapore, 2004).
 - 62) Y. Mori and Y. Okamoto, *J. Phys. Soc. Jpn.* **79**, 074001 (2010).
 - 63) M. Allen and D. Tildesley: *Computer Simulation of Liquids* (Clarendon Press, New York, 1989).
 - 64) H. C. Andersen, *J. Chem. Phys.* **72**, 2384 (1980).
 - 65) S. Nosé, *Mol. Phys.* **52**, 255 (1984).
 - 66) W. Hoover, *Phys. Rev. A* **31**, 1695 (1985).
 - 67) R. Walser, A. E. Mark, and W. F. van Gunsteren, *Chem. Phys. Lett.* **303**, 583 (1999).
 - 68) R. Walser, B. Hess, A. E. Mark, and W. F. van Gunsteren, *Chem. Phys. Lett.* **334**, 337 (2001).
 - 69) H. A. Kramers, *Physica* **7**, 284 (1940).
 - 70) D. K. Klimov and D. Thirumalai, *Phys. Rev. Lett.* **79**, 14 (1997).
 - 71) G. S. Jas, W. A. Eaton, and J. Hofrichter, *J. Phys. Chem. B* **105**, 261 (2001).
 - 72) B. Zagrovic and V. Pande, *J. Comput. Chem.* **24**, 1432 (2003).
 - 73) L. Qiu and S. J. Hagen, *J. Am. Chem. Soc.* **126**, 3398 (2004).
 - 74) S. A. Pabit, H. Roder, and S. J. Hagen, *Biochemistry* **43**, 12532 (2004).
 - 75) P. J. Gee and W. F. van Gunsteren, *Chem.-Eur. J.* **12**, 72 (2005).
 - 76) M. Feig, *J. Chem. Theory Comput.* **3**, 1734 (2007).
 - 77) Y. M. Rhee and V. S. Pande, *J. Phys. Chem. B* **112**, 6221 (2008).
 - 78) G. J. Martyna, M. E. Tuckerman, D. J. Tobias, and M. L. Klein, *Mol. Phys.* **87**, 1117 (1996).
 - 79) S. G. Itoh, T. Morishita, and H. Okumura, *J. Chem. Phys.* **139**, 064103 (2013).
 - 80) M. Matsumoto and T. Nishimura, *ACM Transactions on Modeling and Computer Simulation* **8**, 3 (1998).
 - 81) S. Nosé, *Prog. Theor. Phys. Supp.* **103**, 1 (1991).
 - 82) This may not be the case when the phase transitions are involved.⁹⁴⁾
 - 83) H. Okumura and F. Yonezawa, *J. Chem. Phys.* **113**, 9162 (2000).
 - 84) G. Bussi and M. Parrinello, *Phys. Rev. E* **75**, 056707 (2007).
 - 85) G. E. P. Box and M. E. Muller, *Ann. Math. Stat.* **29**, 610 (1958).
 - 86) B. Efron, *The Jackknife, the Bootstrap, and Other Resampling Plans* (Society for Industrial and Applied Mathematics [SIAM], Philadelphia, 1982).
 - 87) H. Flyvbjerg and H. G. Petersen, *J. Chem. Phys.* **91**, 461 (1989).
 - 88) D. A. McQuarrie, *Statistical Mechanics* (University Science Books, Sausalito, California, 2000).
 - 89) H. J. C. Berendsen, J. P. M. Postma, W. F. van Gunsteren, A. DiNola, and J. R. Haak, *J. Chem. Phys.* **81**, 3684 (1984).
 - 90) T. Morishita, *J. Chem. Phys.* **113**, 2976 (2000).
 - 91) P. H. Hünenberger, *Adv. Polym. Sci.* **173**, 105 (2005).
 - 92) Z. Lin and W. F. van Gunsteren, *J. Chem. Phys.* **143**, 034110 (2015).
 - 93) E. Rosta, N.-V. Buchete, and G. Hummer, *J. Chem. Theory Comput.* **5**, 1393 (2009).
 - 94) E. Bittner, A. Nußbaumer, and W. Janke, *Phys. Rev. Lett.* **101**, 130603 (2008).